NACA RM L54E19a

RESEARCH MEMORANDUM

SOME INTERNAL-FLOW CHARACTERISTICS OF SEVERAL AXISYMMETRICAL NACA 1-SERIES NOSE AIR INLETS AT ZERO FLIGHT SPEED

By Carroll R. Bryan and Frank F. Fleming

Langley Aeronautical Laboratory
Langley Field, Va.

NATIONAL ADVISORY COMMITTEE
FOR AERONAUTICS
WASHINGTON

July 15, 1954
Declassified June 12, 1956

NATIONAL ADVISORY COMMITTEE FOR AERONAUTICS

RESEARCH MEMORANDUM

SOME INTERNAL-FLOW CHARACTERISTICS OF SEVERAL AXISYMMETRICAL NACA 1-SERIES NOSE AIR INLETS AT ZERO FLIGHT SPEED

By Carroll R. Bryan and Frank F. Fleming

SUMMARY

Six NACA 1-series axisymmetrical nose air inlets of 8-inch maximum diameter (one with protruding central body) were tested at zero forward velocity at the Langley 8-foot transonic tunnel. Total-pressure surveys, pressure-recovery measurements, and flow-visualization studies were made through a range of mass-flow ratio extending from below the normal operating range to choking.

Test results showed wide variance in the performance of round-lipped inlets. The two blunter-lipped inlets choked at a mass-flow ratio within 2 percent of the theoretical maximum. There was extensive boundary-layer separation somewhere in the inlet duct at all mass flows. Correlating parameters were found which defined choking mass-flow ratio and maximum choking pressure recovery for the inlets tested to within ±0.02 (nose inlets only) and ±0.01, respectively. These parameters neglected any effect of diffuser geometry.

INTRODUCTION

The design of the internal-flow system of a turbojet-powered aircraft for optimum operation at transonic or supersonic speeds tends to compromise the operation of the system at conditions corresponding to take-off and low-speed operation (i.e., extremely high mass-flow ratios at or very near choking and thus possibly large performance losses). Effort has been made to avoid this low-speed performance penalty in practice by means of auxiliary inlets or by variable-geometry inlets. It would be desirable, of course, to avoid such mechanical complication by the design of a fixed-geometry system having high performance characteristics at mass-flow ratios near the theoretical maximum. However, little information is available on the effects of inlet geometry on static or

low-speed performance (refs. 1 to 5), and, since a transonic inlet investigation in the Langley 8-foot transonic tunnel has made available several 8-inch-diameter subsonic, transonic, and supersonic air inlets of varying proportions and lip profiles, it was considered that a study of the internal performance of these inlets at static conditions might be useful in indicating some of the more important effects of inlet geometry. Although the inlets available did not embody a systematic variation of isolated geometric variables, they do afford a wide range of the variables of lip roundness, inlet area, and diffusion rate and magnitude. Accordingly, static induction tests of several of these inlets were conducted on a suction test stand at the Langley 8-foot transonic tunnel.

In this paper the results of the static-condition investigation of six NACA 1-series nose inlets (one with protruding central body) are reported and compared with other data available. Total-pressure surveys and pressure-recovery measurements were made through a mass-flow range extending from below the normal operating range to choking. In addition, flow-visualization studies were made of some of the inlets by utilizing the tuft and the liquid-film-flow techniques.

SYMBOLS

A	duct cross-sectional area
D	maximum body diameter, 8.0
H	total pressure
$\overline{H}$	average total pressure, $\int H \frac{dA}{A}$
m	mass-flow rate
m/m_s	mass-flow ratio, $\frac{\rho VA}{\rho_s V_s A_{min}}$
M	Mach number
p	static pressure
P_a	atmospheric pressure
m/m_{ch}	relative mass-flow ratio, $\frac{m/m_s}{(m/m_s)_{ch}}$
r	radius

r_l	local duct radius
R	body maximum radius, D/2
V	velocity
x	axial distance, positive downstream
X	axial distance between the inlet plane and the duct minimum-area station
y	radial distance from reference line (see fig. 2), positive toward model axis
Y	inner-lip thickness at duct minimum-area station
ρ	mass density
ϕ	diffuser equivalent conical angle

Subscripts:

i	inlet plane
ch	condition corresponding to choking at duct minimum-area station
min	inlet duct minimum-area station (see fig. 1)
s	condition corresponding to a Mach number of 1.0 for isentropic flow
2	inlet duct maximum-area station (diffuser-exit station)

APPARATUS AND TESTS

Models.- Figure 1 presents schematic drawings of the various inlet shapes tested and gives some design details of these inlets. Further details of the inlet profile and design of these inlets may be found in reference 6. The NACA 1-70-200 nose inlet was constructed of Fiberglas-Paraplex laminate. The other nose inlets were of spun-aluminum construction throughout. The two internal central bodies used in the nose-inlet tests and the tube supporting the protruding central body in the NACA 1-80-300 configuration were also of spun-aluminum construction. The protruding central body was of wood construction surfaced with Paraplex plastic. The inlet inner-lip contours (ellipses all, followed by a

cylindrical section) are defined in figure 2, and the inlet-duct-area variations from the inlet lip to the diffuser-exit station are shown in figure 3. The inner-lip contours are compared in figure 4, scaled to the same inlet diameter.

Apparatus.- A schematic drawing of the test apparatus is presented in figure 5. The inlets were mounted on a long steel barrel which housed the diffuser-exit rakes and a venturi tube containing a rake of static- and total-pressure tubes. The low-pressure source was a 10,000 cu-ft/min compressor.

Flow visualization.- For flow-visualization purposes, two inlets, the NACA 1-40-200 and 1-70-200, were fitted with 1/8-inch steel plates constructed to extend along the model center line from well in front of the model to $4\frac{1}{2}$ inches into the inlet and to conform closely to the model-inner-wall contour. A drawing of one of these plates is shown in figure 6. The flow patterns were obtained by brushing with one stroke a thin mixture of Varsol and commercial Prussian blue oil pigment around the region of the inlet while the inlet was operating at the desired mass flow. When the pigment had dried enough to stop flowing, the compressor was shut down, the flow-plate removed, and the pattern photographed.

Tufts used in other flow-visualization studies were 3/4-inch lengths of braided nylon cord secured to the model with clear dope. Tuft observations were photographed at 64 frames per second.

Tests and measurements.- The inlets were mounted on the steel barrel together with the appropriate fairing. The back pressure was reduced through several intermediate steps until the inlet was choked. The back pressure was then further reduced to increase the internal losses and to define adequately the choking mass-flow ratio. At each step, static- and total-pressure readings from the diffuser-exit and venturi rakes (and when present, from a small survey rake located on the outer duct wall 5 inches behind the inlet plane) were photographically recorded from a multitube manometer board.

The relative areas were such that the venturi tube choked at a lower mass flow than did the NACA 1-60-200 and 1-70-200 nose inlets. Two further tests were then made of the NACA 1-70-200 nose inlet with the venturi tube removed. This inlet was tested to define completely the choking mass-flow ratio and was also tested with a transition strip located on the inlet inner lip. The transition strip, covering the entire annulus of the inlet and consisting of number 60 carborundum grains cemented to the model surface with clear lacquer, extended from the leading edge of the inlet 3/4 inch into the inlet.

For those tests where the venturi tube was present both mass-flow ratio and average total-pressure ratio were calculated from the readings of the venturi rake. Although separated flow, as is shown subsequently, was always present at the diffuser-exit station, it was interesting to note that the average total-pressure ratio measured at this station was within 1 percent of that measured at the venturi station. Computations of mass-flow ratio and average total-pressure ratio for the NACA 1-70-200 nose inlet were, since the venturi tube was not present, made from readings of the diffuser-exit rakes. Inasmuch as comparison of mass-flow-ratio computations for the NACA 1-40-200 and 1-50-200 nose inlets indicated that values of mass-flow ratio computed from the diffuser-exit rakes were considerably higher than those from the venturi rake, it may be assumed that the values presented for the 1-70-200 inlet are likewise considerably in error.

The accuracy of the measurements is estimated as: mass-flow ratio measured at the venturi station, +0.02, or -0 (no estimate is made for the NACA 1-70-200 nose inlet); total-pressure ratio, ±0.01; and average total-pressure ratio, ±0.01.

RESULTS AND DISCUSSION

Total-pressure profiles.- The effects of mass-flow ratio on the total-pressure profiles for several of the inlets are shown in figures 7 to 10. For most cases, the diffuser-exit profiles were of unfavorable types associated with flow separation from the outer duct wall. Generally, the flow at the diffuser-exit station became more asymmetric at the higher mass-flow ratios.

There was a wide latitude in the shapes of the total-pressure profiles at the 5-inch station, and furthermore the shapes would frequently change very noticeably with no change in the compressor setting. However, for all cases where there was no supersonic flow past this station, the profiles indicated boundary-layer separation. The one profile which showed supersonic flow past this station was at a m/m_s of 0.87 for the NACA 1-70-200 inlet (see fig. 9(a)). At this condition, the back pressure had been reduced sufficiently to pull the strong shock and its accompanying boundary-layer separation down past the 5-inch station.

Flow visualization.- The photographs of tuft observations and of ink-flow patterns shown in figures 11 and 12 were selected to show typical examples of tuft and ink-flow patterns obtained. The drawings of figure 13 are presented to illustrate more clearly some of the types of flow phenomena observed in the photographs of figure 12.

Tuft observations of the NACA 1-60-200, 1-70-200, and 1-50-400 nose inlets indicated the presence of flow separation at or close to the inlet lip for all conditions except that of supersonic flow preceding a strong shock inside the inlet. At this condition, attached flow existed back to the shock where separation then occurred. Flow at all conditions below choking exhibited signs of extreme roughness (extreme agitation of tufts in immediate vicinity of inlet plane, large regions of separated flow shifting around the duct irregularly, and loud aural phenomena characteristic to each inlet). The examples of tuft pictures shown in figure 11 are consecutive frames from a study of the NACA 1-60-200 nose inlet at a mass-flow ratio of approximately 0.80. Separation from the region of the leading edge is evident in these pictures. This example was selected to show the roughness in the inlets at high mass-flow ratios near choking. The flow at the inlet entrance can be seen to vary widely in character in the short space of 40 frames. The tube protruding from the inlet is a static pressure probe coinciding with the inlet center line.

Generally, the lines in the ink-flow patterns of figure 12 tend to represent streamlines where the boundary layer of the plate was very thin and there was no crossflow or strong lateral pressure gradient. They tend to represent motion within the boundary layer on the flow plate where this boundary layer was thick or where there were strong lateral pressure gradients, as near the lips (point Ⓐ, fig. 13). It must be remembered therefore that the patterns shown are not an exact representation of the flow encountered in an impediment-free inlet. The flow plate was present, and its boundary layer undoubtedly had some effect on inlet flow. At all mass-flow ratios below choking, the ink-flow patterns for the NACA 1-40-200 nose inlet are very similar. The area of heavy streaks (point Ⓓ, fig. 13) indicates that transition on the duct wall was very close to the inlet plane. The duct-wall boundary layer, though exceedingly turbulent and possibly separated, was not of significant thickness until the minimum section was passed, where extensive boundary-layer separation occurred (point Ⓒ, fig. 13). As the mass-flow ratio was raised to just below choking, the boundary-layer thickness grew slightly and the area of separation extended over a larger portion of the plate. These areas of boundary-layer separation seen in all the figures are probably much larger than those found in an impediment-free inlet because of the interaction of the plate and duct-wall boundary layers.

As the inlet choked, a strong shock formed, showing as a dark line (fig. 12) followed by a region much lighter than that preceding the shock (illustrated by point Ⓑ, fig. 13). Separation behind this shock was extensive; tuft observations and the diffuser-exit profiles of figure 7 corroborate the evidence in figures 12(b) and (c) that separation caused extreme nonuniformities in the profiles at the diffuser-exit station for this configuration (see $m/m_s = 1.00$, fig. 7). Furthermore, the crossing of the streamlines in figure 12(b) offers evidence which indicates that

this region of separated flow oscillated back and forth irregularly in the duct; this phenomenon also was observed with tufts.

Pronounced boundary-layer separation may be seen at the immediate vicinity of the inlet lip at all subchoking mass flows for the NACA 1-70-200 nose inlet (point Ⓔ, fig. 13). The crossing of the streamlines at the lip for a mass-flow ratio of 0.30 showed the unsteadiness of the flow even at this low flow rate. Boundary-layer separation was so severe for this inlet that downstream from the 3-inch station ($m/m_s = 0.30$), no ink flowed in the separated region near the wall. Increasing the mass-flow ratio to choking resulted, as for the 1-40-200 inlet, in attached flow back to the position of the strong shock where separation then occurred. The shock pattern was less obvious from the ink-flow studies of this inlet because of the extreme turbulence of the flow. All the ink-flow patterns indicate that, outside the inlet, the velocity of the entering air decayed rapidly from the inlet plane. Local Mach numbers along the external surface of the NACA 1-50-200 nose inlet, determined from static-pressure surveys (not presented), showed flow velocities at the choking condition of only $M \approx 0.09$ at 3/4 inch from the plane of the inlet; thus, the internal-flow characteristics were essentially independent of the external shape of the inlet.

Pressure recovery.- The variation of average total-pressure ratio with mass-flow ratio is shown in figure 14. Choking mass-flow ratio for the NACA 1-40-200 and 1-50-200 inlets was within about 2 percent of the theoretical maximum, and average total-pressure ratios at choking were considerably above those for the other inlets. The agreement of the pressure-recovery curves for the NACA 1-70-200 nose inlet with and without leading-edge transition strip (see fig. 15) is presumed to indicate the presence of a turbulent or separated boundary layer at or very close to the leading edge. This belief is borne out by the ink-flow patterns of figure 12 which show separation or transition of the boundary layer within 1 inch of the leading edge at all mass flows for both this inlet and the 1-40-200.

In order to check the accuracy of the extremely high values of mass-flow ratio obtained for the blunter-lipped inlets, a static-pressure survey of the duct minimum-area station was conducted for the NACA 1-50-200 nose inlet at the choking condition. The results of this survey are presented as local Mach number in figure 16(a) and as point-mass-flow ratio in figure 16(b). Although the Mach numbers shown may seem high for efficient mass flow, the variation of ρV with Mach number near a Mach number of unity is such that even at a Mach number of 1.3, for instance, mass flow is still 94 percent of the maximum attainable. Thus, an integration of the point-mass-flow curve (fig. 16(b)) gave a value of choking mass-flow ratio of 0.97, which agreed well with the value 0.98 obtained from the venturi measurements.

Effect of lip geometry.- The variation of average total-pressure ratio with relative mass-flow ratio m/m_{ch} is presented in figure 17. Performance characteristics of the inlets of reference 7 are also compared in this and the following figures. When the inlet performance is presented as in figure 17, it is possible to compare more directly the pressure recovery characteristics of the various configurations. In an effort to achieve some degree of correlation of the geometric variables of the inlets considered, figure 18 was prepared, in which the variation of maximum choking total-pressure ratio and choking mass-flow ratio with the inlet-entrance area-contraction ratio is presented. This parameter is the ratio of the flow area at the duct minimum section to that at the inlet plane. It is to be noted that, with the exception of the 1-80-300 point, this parameter defines the choking mass-flow ratio to within ±2 percent of the arbitrary curve shown. The NACA 1-80-300 inlet configuration differed in type from the other inlets in that it alone of all the round-lipped inlets had a protruding central body.

An expression which correlates the choking pressure-recovery data with more success is the lip-roundness parameter XY/r_i^2. Maximum choking total-pressure ratio and total-pressure ratio for $m/m_s = 0.90$ are presented as a function of this lip-roundness parameter in figure 19. This parameter defines the pressure recovery at choking to within ±0.01 and to within ±0.015 at $m/m_{ch} = 0.90$ (this spread includes the 1-80-300 points). It must be remembered, however, that the inlet diffusers varied widely, and that the effects of this variation on pressure recovery are unfortunately included in the above correlation. Just how strong these effects were could not be determined because of the nonsystematic variation of the geometric parameters, but it can be pointed out that two inlets having quite different diffusers (the NACA 1-40-200 nose inlet had a diffuser angle of 14.4° while the open-nose conical inlet with bell lip had a diffuser angle of only 4.4°) had similar lip-roundness parameters and similar choking pressure recovery (see fig. 19).

CONCLUDING REMARKS

Six NACA 1-series axisymmetrical nose air inlets of 8-inch maximum diameter (one with protruding central body) were tested at zero forward velocity in the Langley 8-foot transonic tunnel. From the results of this investigation, the following observations were made:

Performance characteristics of inlets having differing amounts of roundness varied widely. The two blunter-lipped inlets choked at a value of mass-flow ratio within 2 percent of the theoretical maximum.

All the inlets tested showed boundary-layer separation from a large portion of the duct wall beginning at or near the inlet lip for all mass flows below choking. Despite the presence of these regions of separated flow, some correlating geometric parameters were found which defined, for the inlets of this investigation and those of a similar investigation reported in reference 7, choking mass-flow ratio to within ±0.02 (nose inlets only) and choking maximum average total-pressure ratio to within ±0.01. These parameters neglected any effect of diffuser geometry.

Langley Aeronautical Laboratory,
National Advisory Committee for Aeronautics,
Langley Field, Va., May 10, 1954.

REFERENCES

1. Seddon, J., and Trebble, W. J. G.: Experiments on the Flow Into a Swept Leading Edge Intake at Zero Forward Speed With Notes on the Wider Uses of a Slotted Intake. Rep. No. Aero. 2409, British R.A.E., Jan. 1951.

2. Seddon, J., and Kettle, D. J.: Low Speed Wind Tunnel Tests on the Characteristics of Leading Edge Air Intakes in Swept Wings. Rep. No. Aero. 2402, British R.A.E., Nov. 1950.

3. Seddon, J., and Raney, D. J.: Low Speed Wind Tunnel Model Tests of Submerged Air Intakes on the Undersurface of a Delta Wing. Rep. No. Aero. 2428, British R.A.E., 1951.

4. Watson, Earl C.: Some Low-Speed Characteristics of an Air-Induction System Having Scoop-Type Inlets With Provisions for Boundary-Layer Control. NACA RM A51F15, 1951.

5. Holzhauser, Curt A.: The Effect of Entrance Mach Number and Lip Shape on the Subsonic Characteristics of a Scoop-Type-Air-Induction System for a Supersonic Airplane. NACA RM A51J19a, 1952.

6. Pendley, Robert E., Milillo, Joseph R., and Fleming, Frank F.: An Investigation of Three NACA 1-Series Nose Inlets at Subsonic and Transonic Speeds. NACA RM L52J23, 1953.

7. Milillo, Joseph R.: Some Internal-Flow Characteristics at Zero Flight Speed of an Annular Supersonic Inlet and an Open-Nose Inlet With Sharp and Rounded Lips. NACA RM L54E19, 1954.

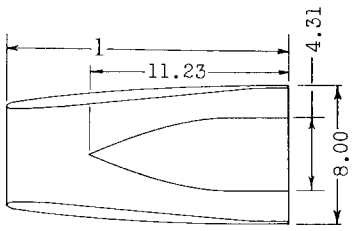

NACA 1-70-200 nose inlet

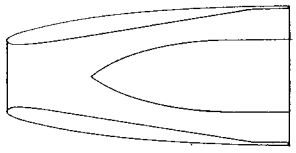

NACA 1-50-200 nose inlet

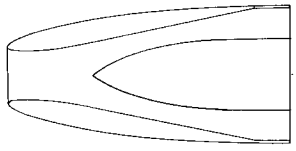

NACA 1-40-200 nose inlet

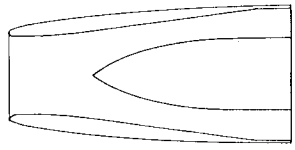

NACA 1-60-200 nose inlet

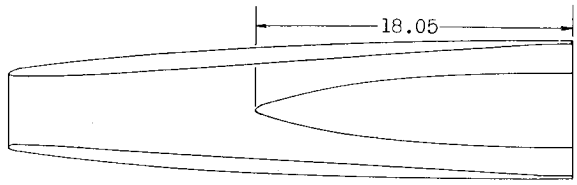

NACA 1-50-400 nose inlet

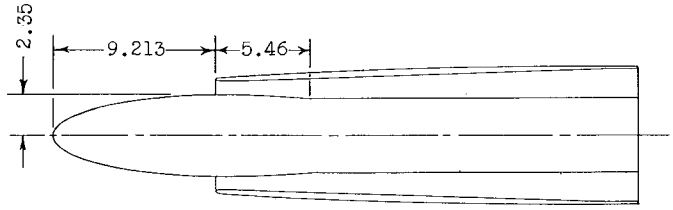

NACA 1-80-300 nose inlet
with elliptical central body

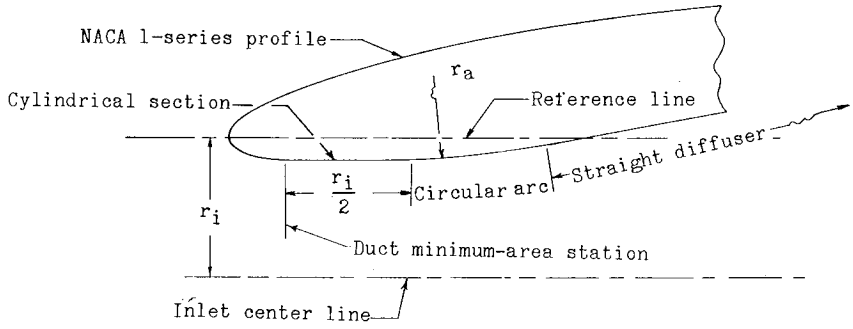

NACA Nose-Inlet Design Details

	1-70-200	1-50-200	1-40-200	1-60-200	1-50-400	1-80-300
r_i	2.83	2.05	1.61	2.44	2.05	3.22
r_a	30.69	22.25	15.05	20.50	62.50	52.75
l	16.00	16.00	16.00	16.00	32.00	24.00
$A_{min.}$	23.072	10.869	6.157	16.048	11.946	13.267
r_{min}	2.71	1.86	1.40	2.28	1.95	2.055*

*Based on a circle equal in area to A_{min}

Figure 1.- Inlet profiles tested.

INNER-LIP COORDINATES

All coordinates in inches

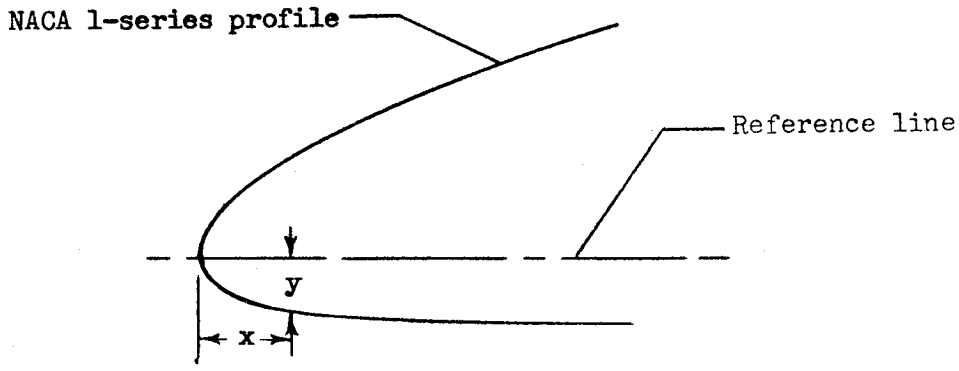

NACA 1-40-200 nose inlet

x	y
0.000	0.000
.100	.129
.200	.171
.300	.195
.400	.207
.469(X)	.209(Y)
1.299	.209

leading-edge radius 1.609

NACA 1-50-200 nose inlet

x	y
0.000	0.000
.069	.100
.169	.145
.269	.170
.369	.182
.469(X)	.186(Y)
1.493	.186

leading-edge radius 2.0465

NACA 1-50-400 nose inlet

x	y
0.000	0.000
.053	.064
.133	.091
.218(X)	.094(Y)

leading-edge radius 2.049

NACA 1-60-200 nose inlet

x	y
0.000	0.000
.069	.080
.169	.118
.269	.139
.369	.150
.469(X)	.154(Y)
1.689	.154

leading-edge radius 2.439

NACA 1-70-200 nose inlet

x	y
0.000	0.000
.100	.075
.200	.099
.300	.113
.400	.120
.469(X)	.121(Y)
1.884	.121

leading-edge radius 2.829

NACA 1-80-300 nose inlet

x	y
0.000	0.000
.050	.032
.100	.043
.200	.054
.300	.064
.400(X)	.067(Y)
2.042	.067

leading-edge radius 3.220

Figure 2.- Coordinates of inner-lip fairings. All dimensions are in inches.

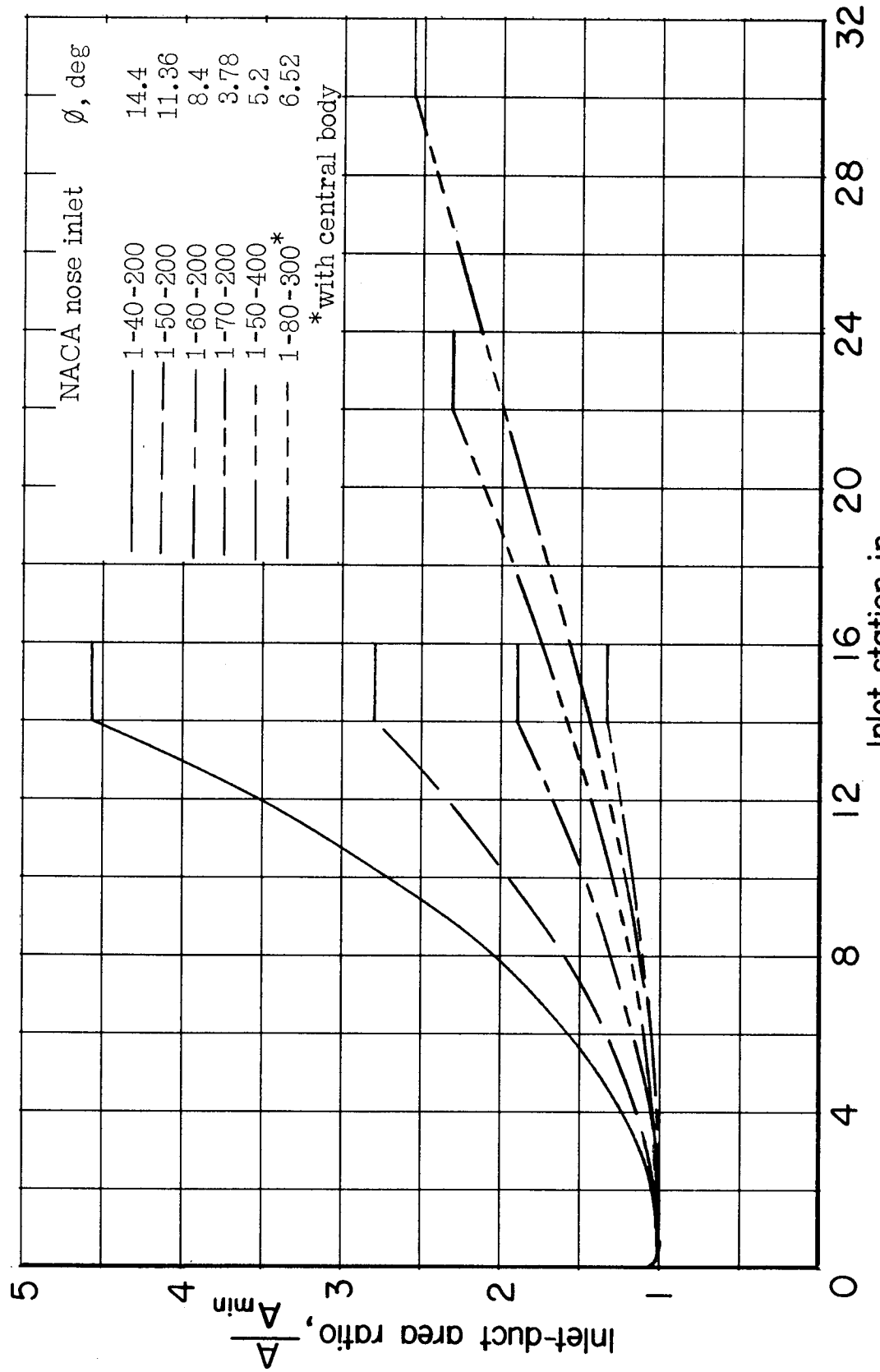

Figure 3.- Variation of inlet-duct area.

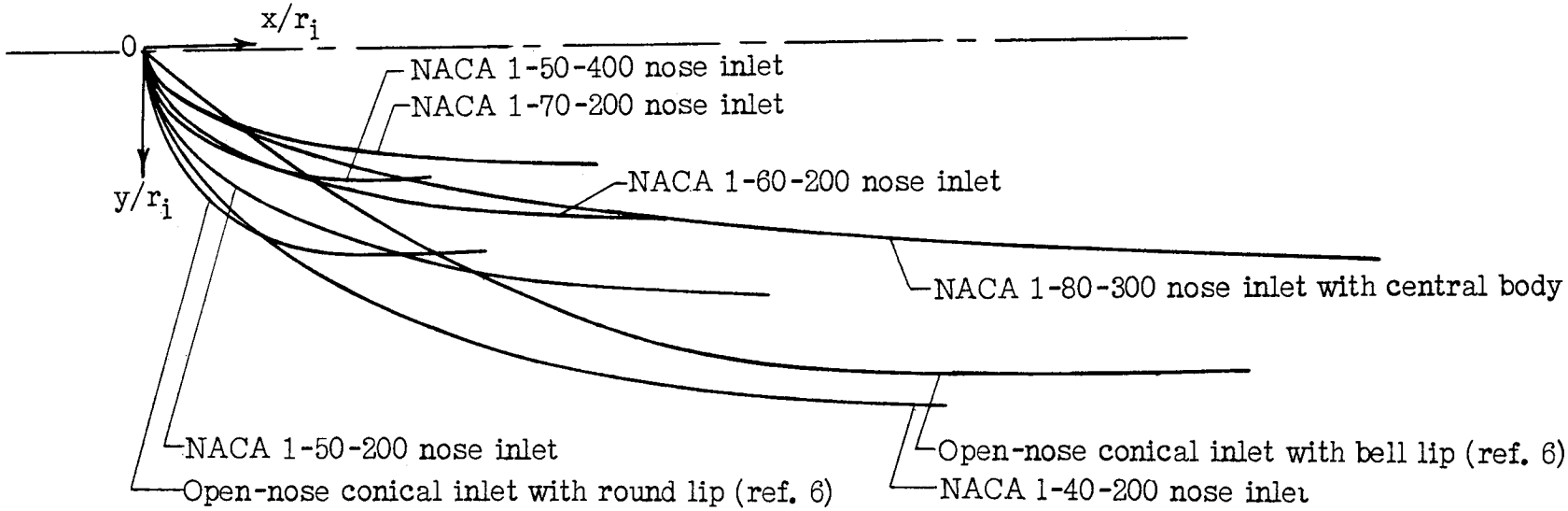

Figure 4.- Inner-lip-shape comparison based on common inlet radius r_i.

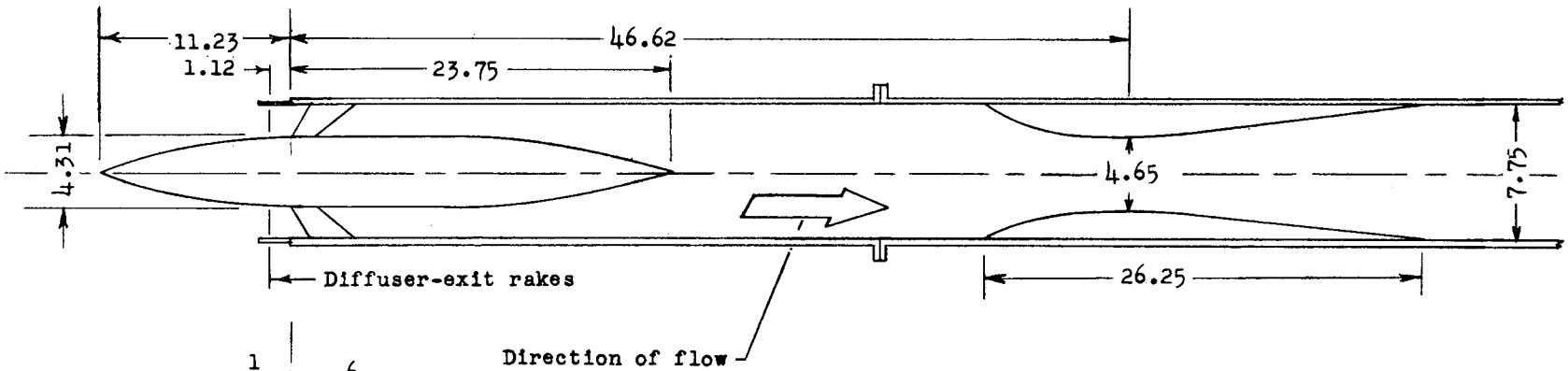

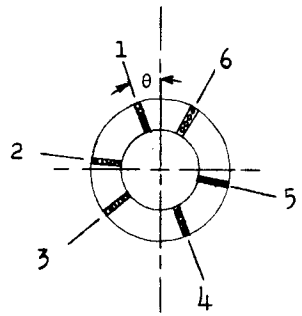

Diffuser-exit station

Diffuser-exit rake position

Rake	θ, deg
1	24
2	84
3	134
4	204
5	265
6	315

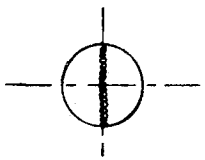

Venturi rake

Figure 5.- Details of static test mount. All dimensions are in inches.

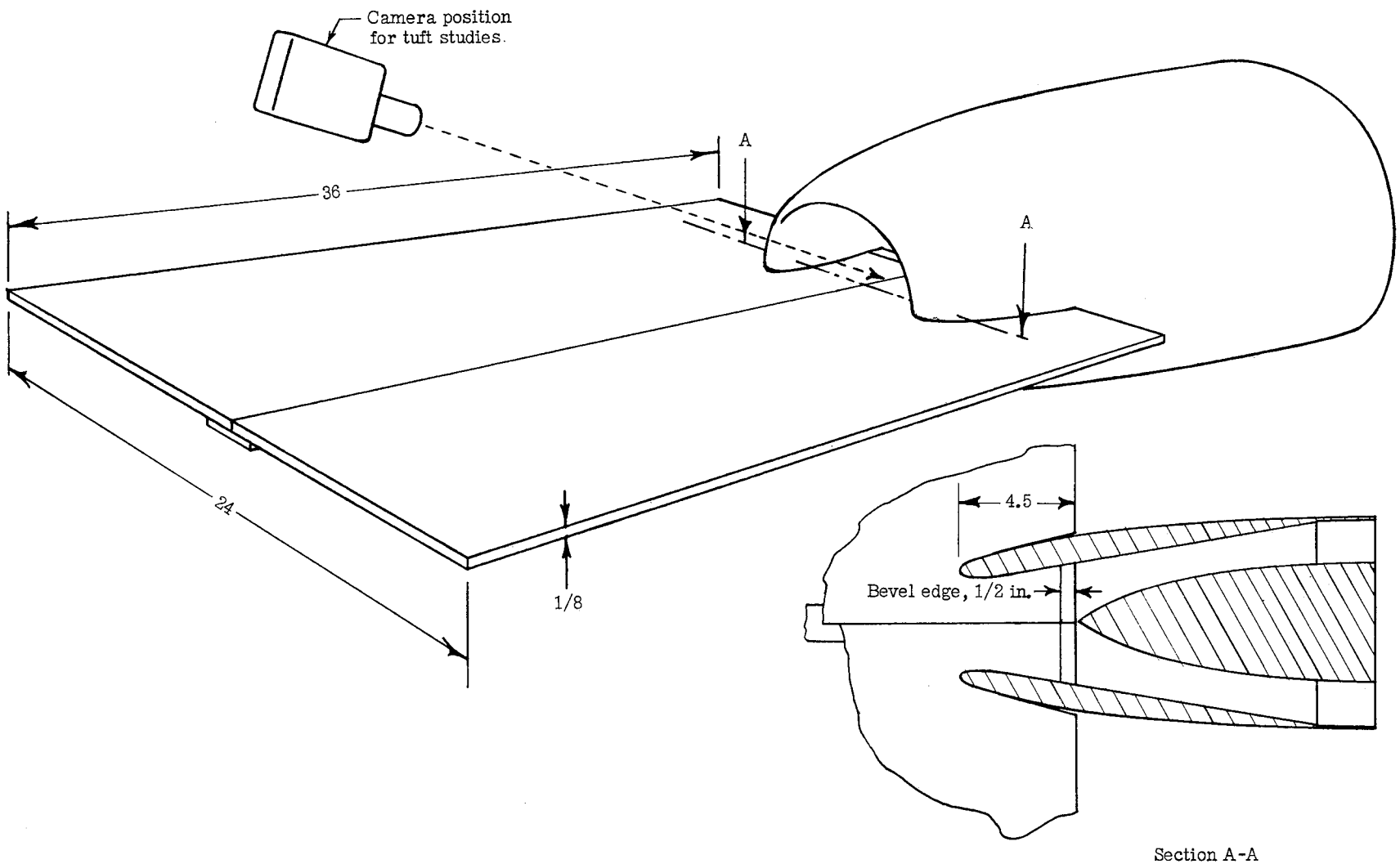

Figure 6.- Flow-visualization plate. All dimensions are in inches.

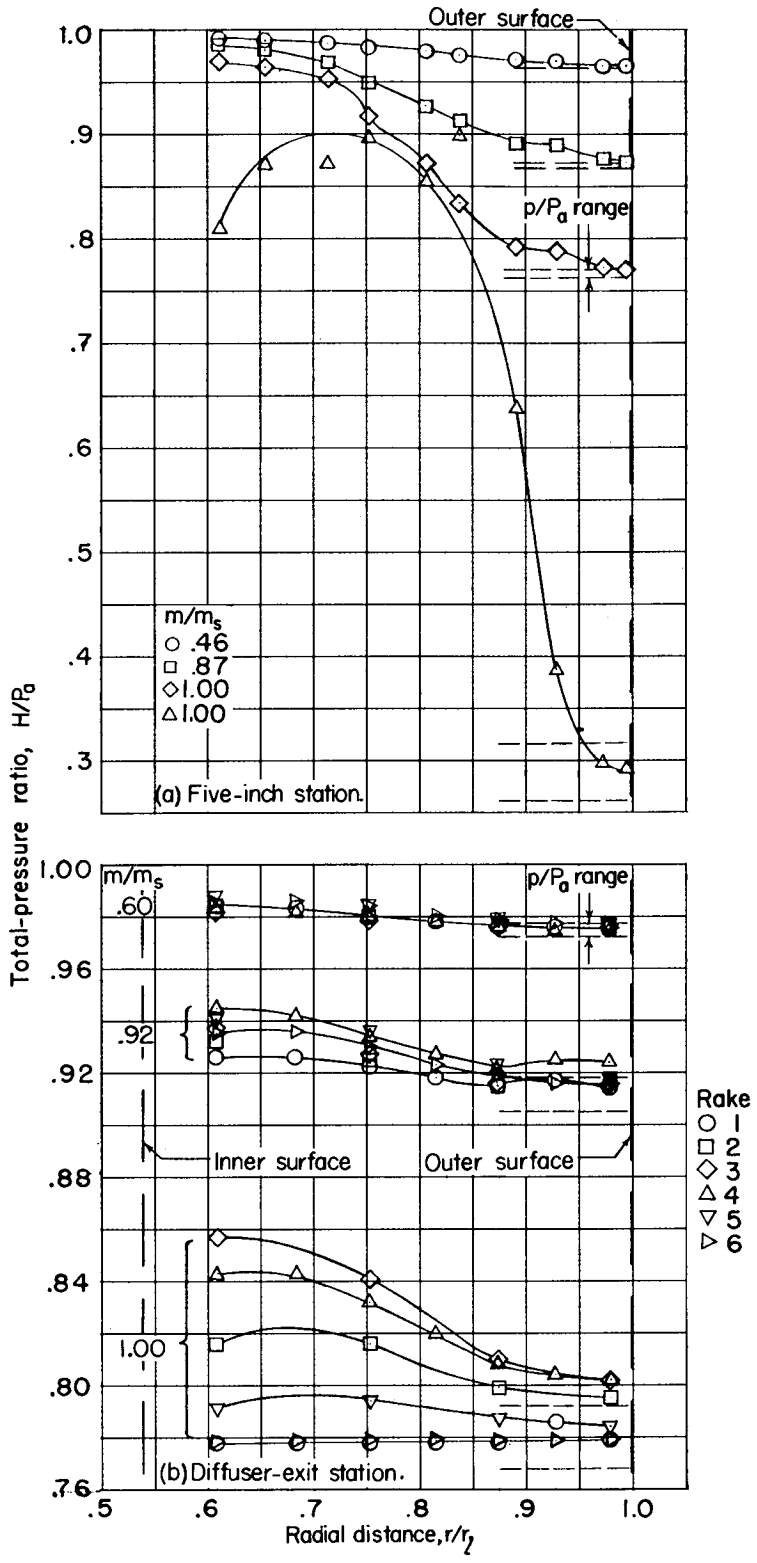

Figure 7.- Total-pressure-ratio variation with radial distance; NACA 1-40-200 nose inlet. Duct radius at 5-inch station is 1.85 inches.

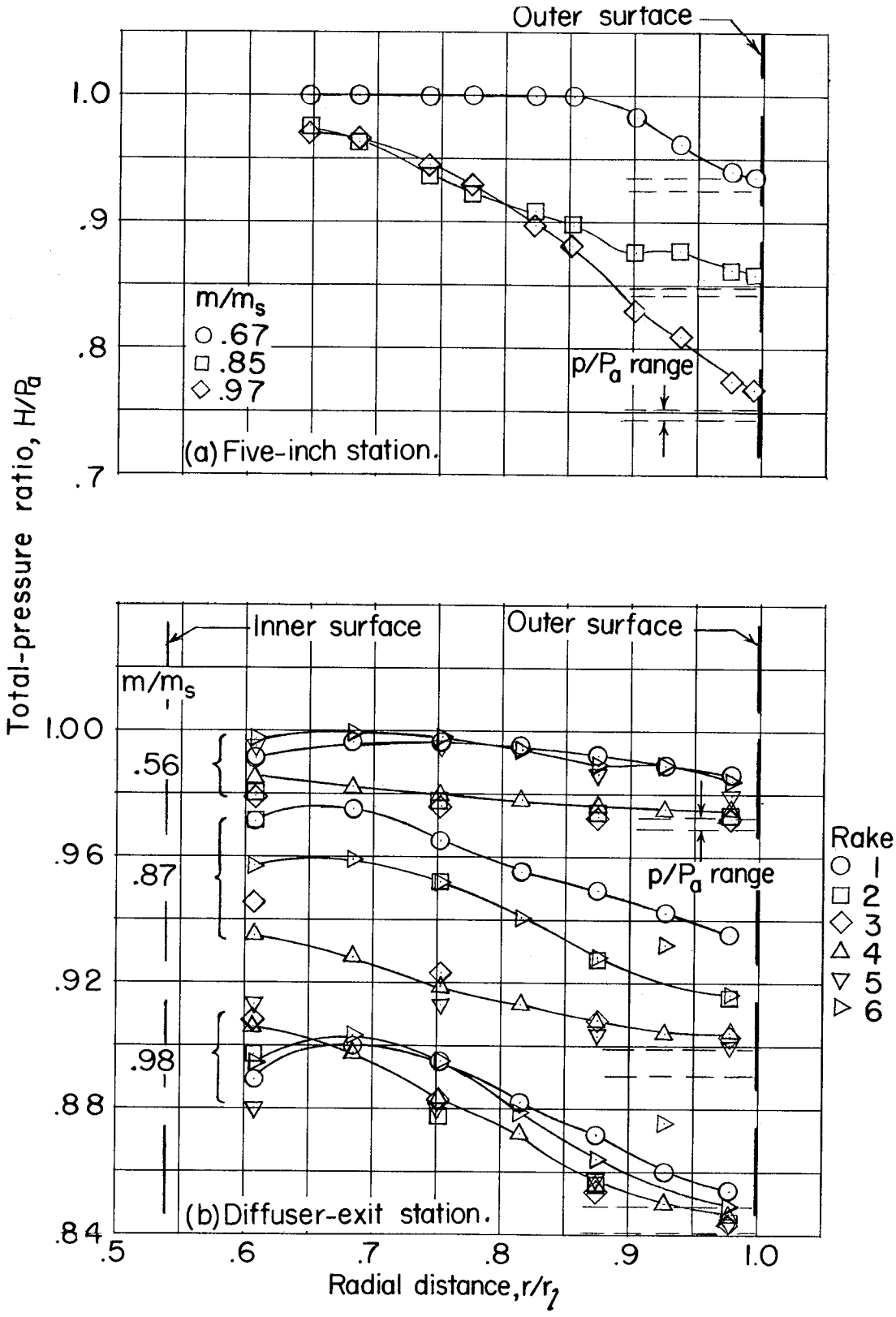

Figure 8.- Total-pressure-ratio variation with radial distance; NACA 1-50-200 nose inlet. Duct radius at 5-inch station is 2.08 inches.

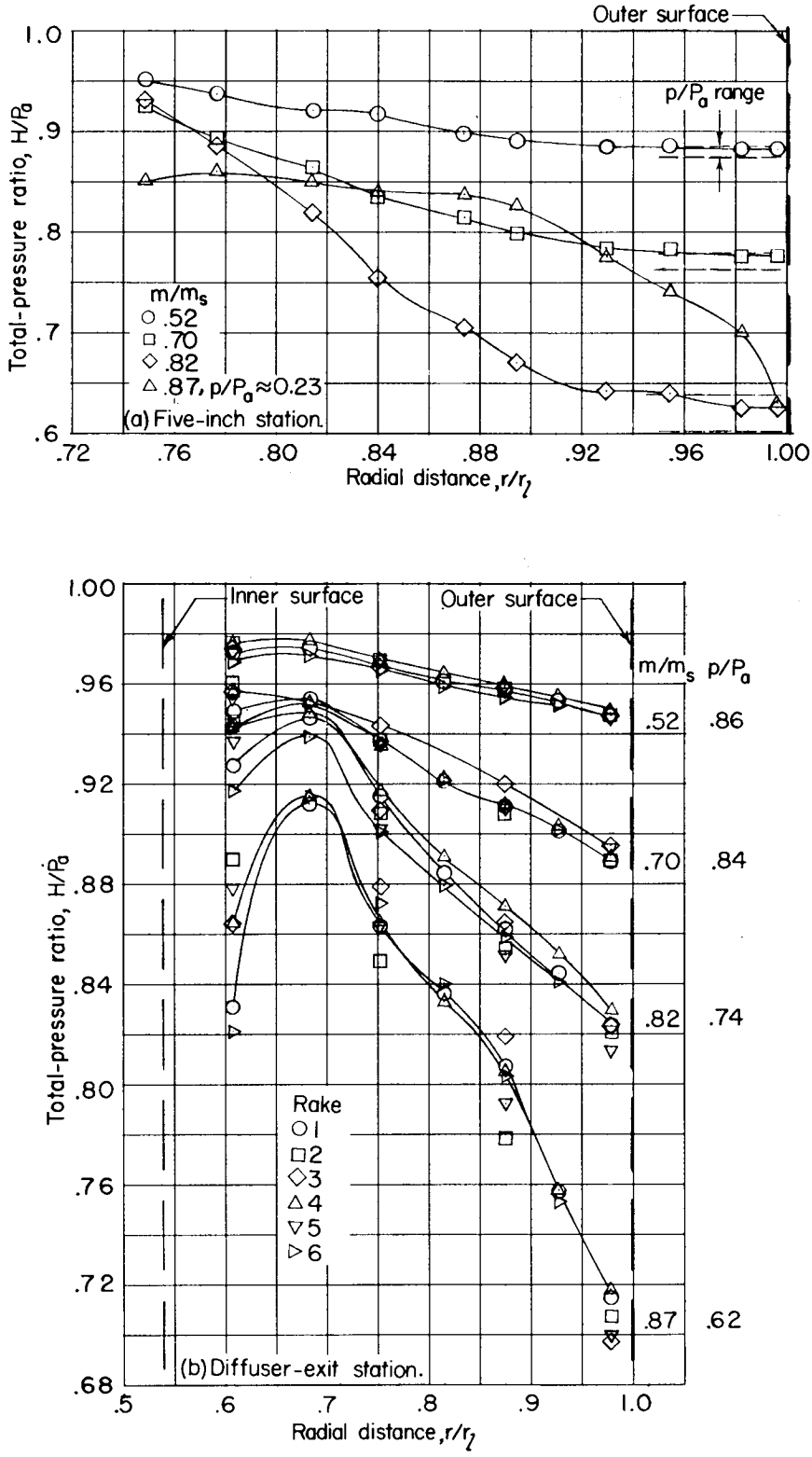

Figure 9.- Total-pressure-ratio variation with radial distance; NACA 1-70-200 nose inlet. Duct radius at 5-inch station is 2.86 inches.

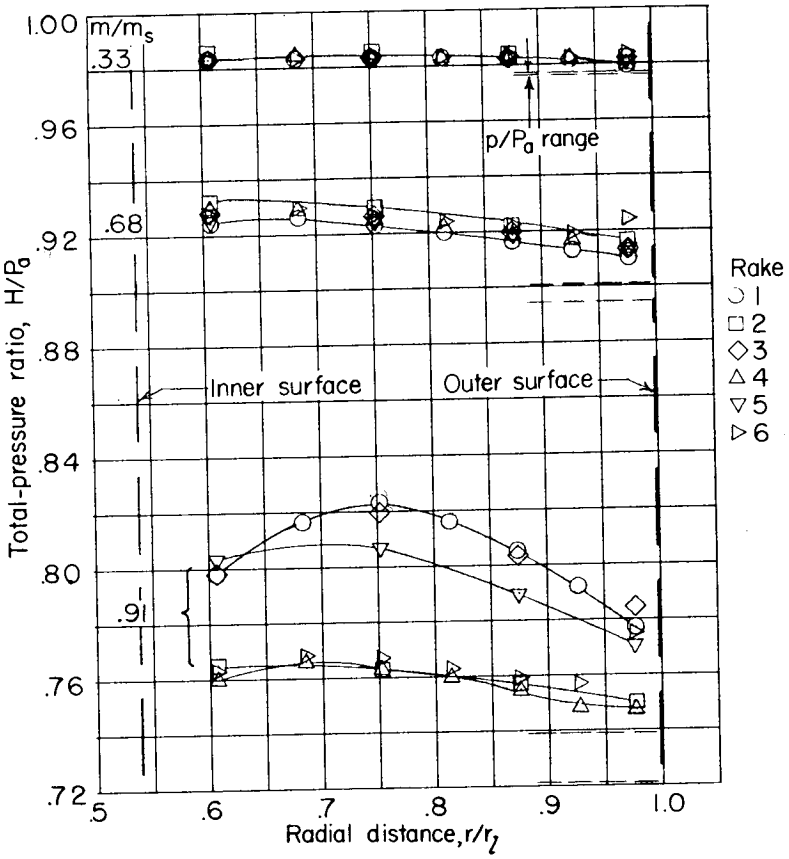

(a) NACA 1-80-300 nose inlet with elliptical central body.

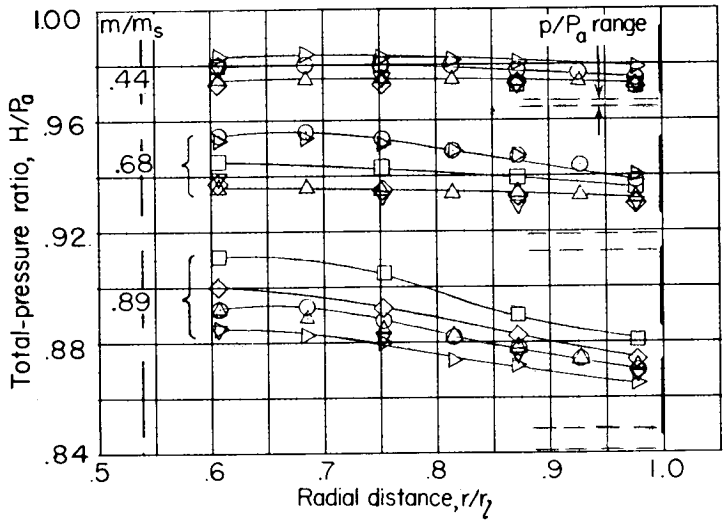

(b) NACA 1-50-400 nose inlet.

gure 10.- Variation with radial distance of total-pressure ratio at the diffuser-exit station.

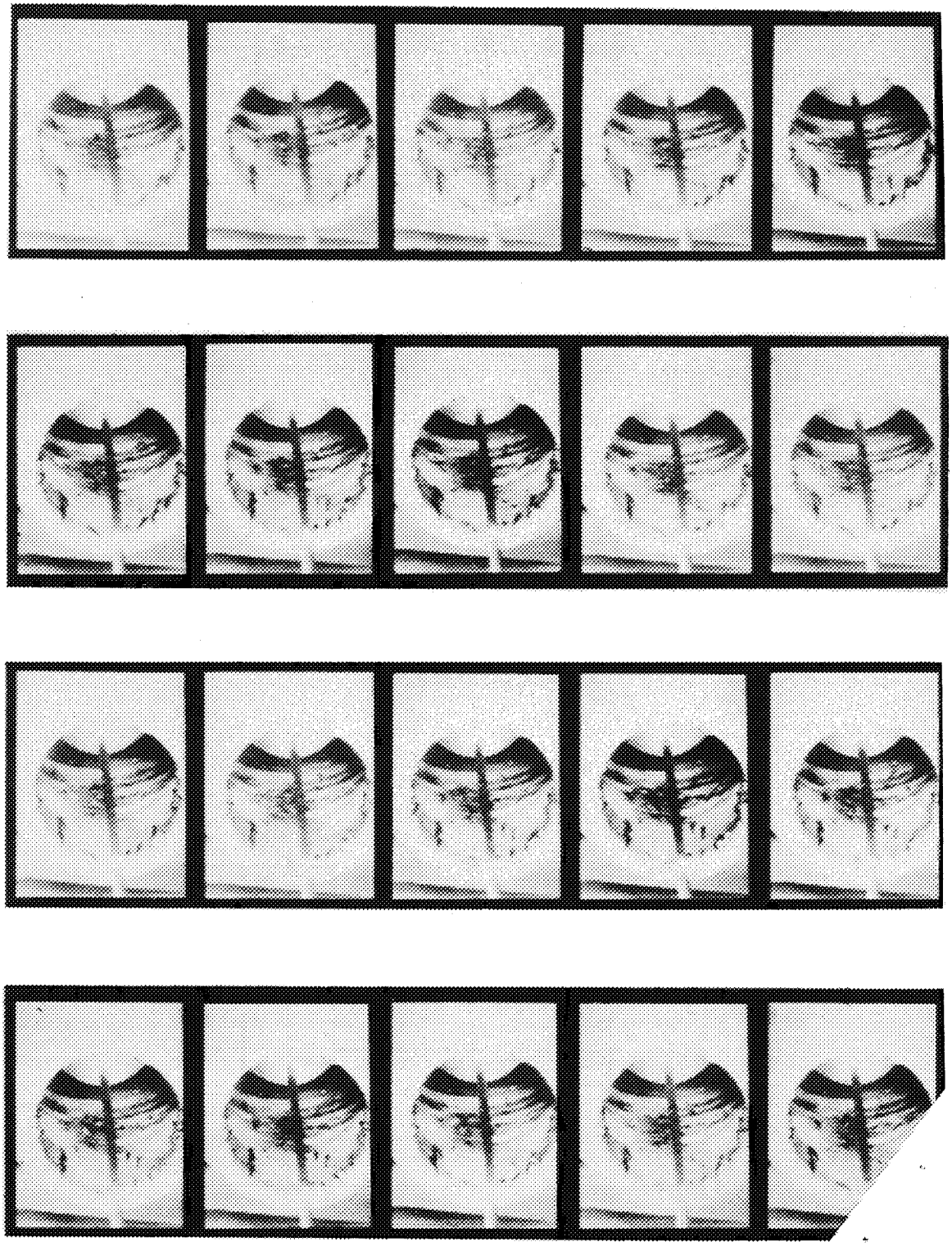

(a) Frames 1 to 20.

Figure 11.- Tuft photographs. NACA 1-60-200 nose inlet; m_1

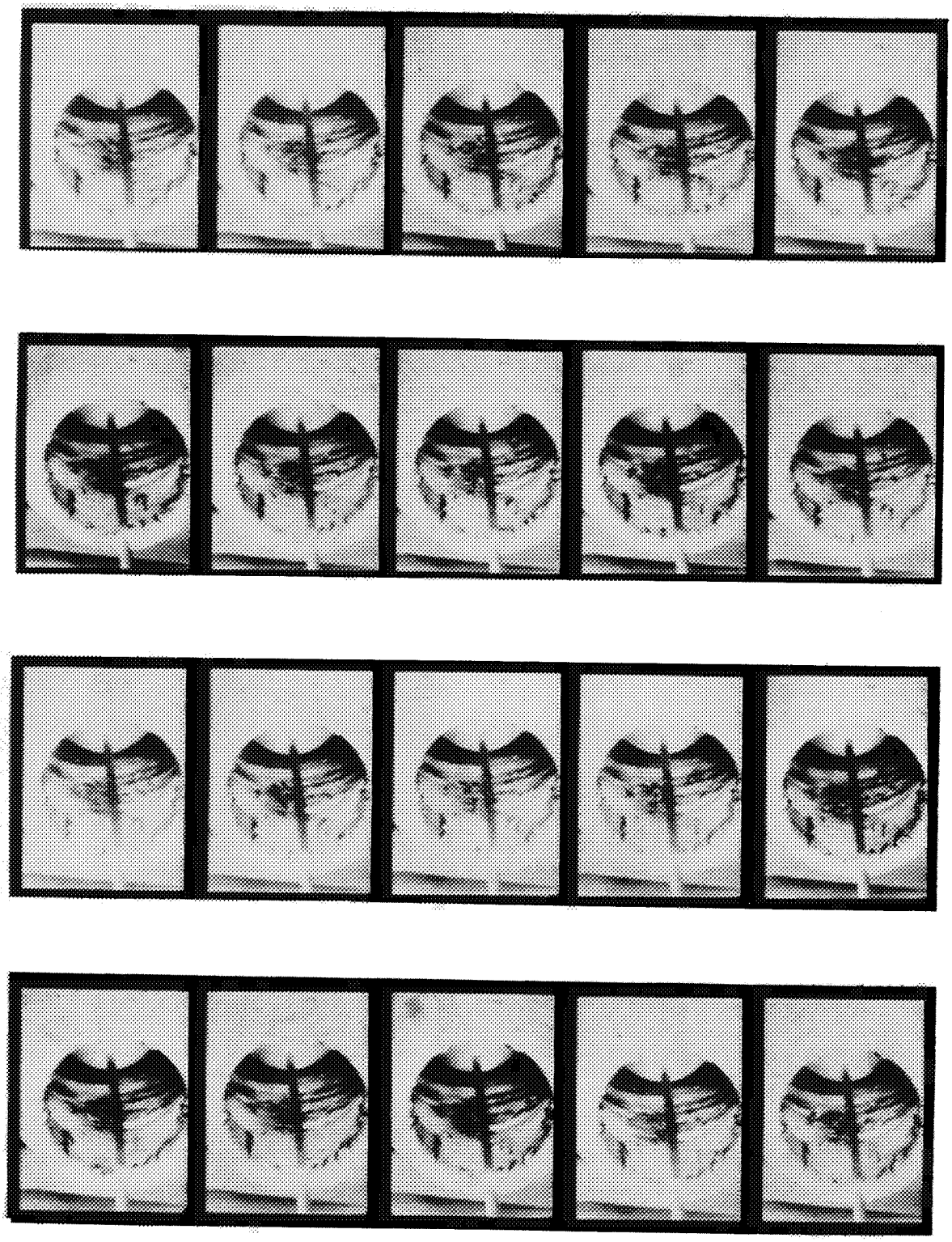

(b) Frames 21 to 40. L-83680

Figure 11.- Concluded.

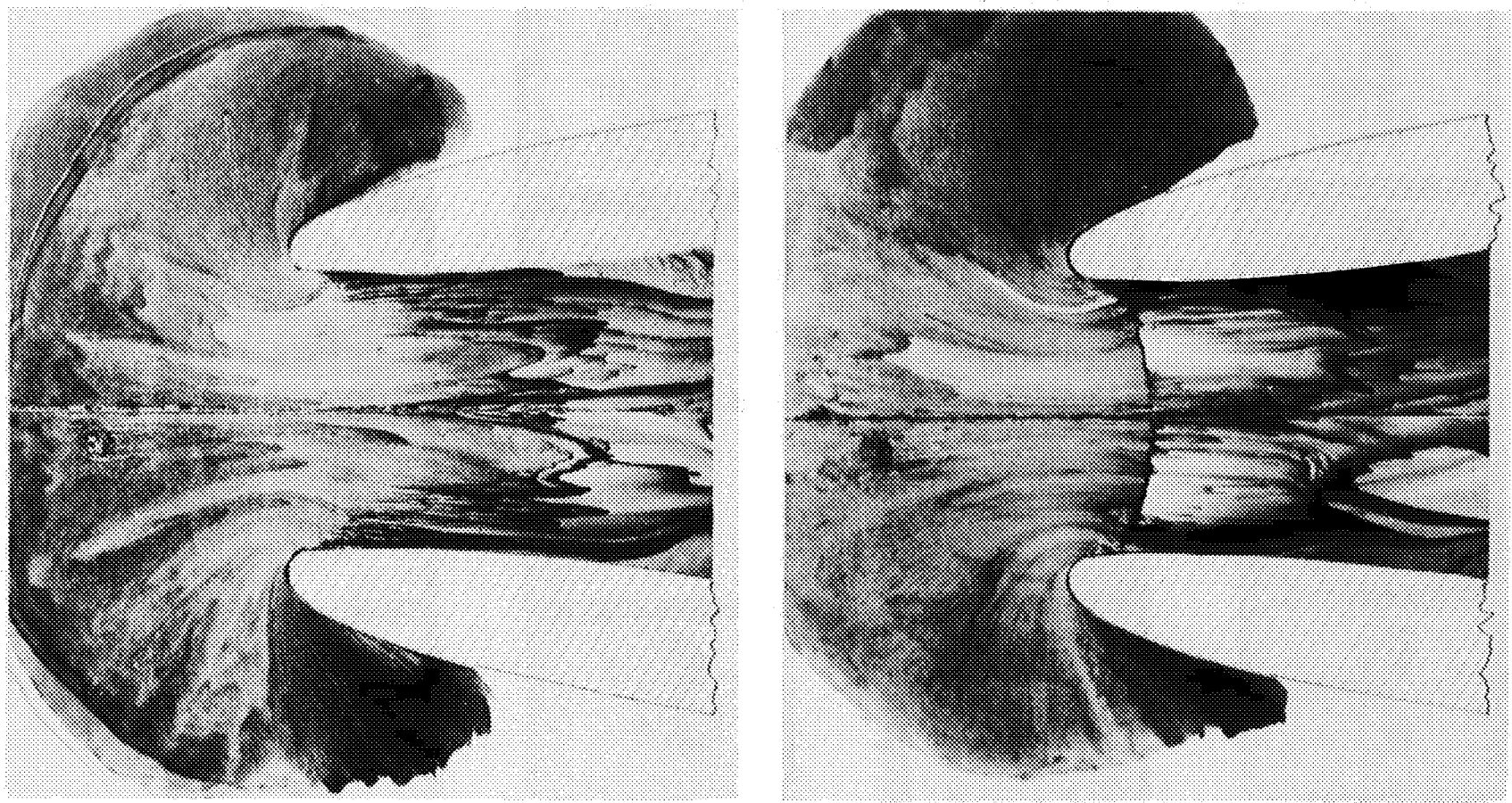

L-83681

(a) NACA 1-40-200 nose inlet, $m/m_s \approx 0.48$.

(b) NACA 1-40-200 nose inlet, m/m_s = choke.

Figure 12.- Ink-flow patterns.

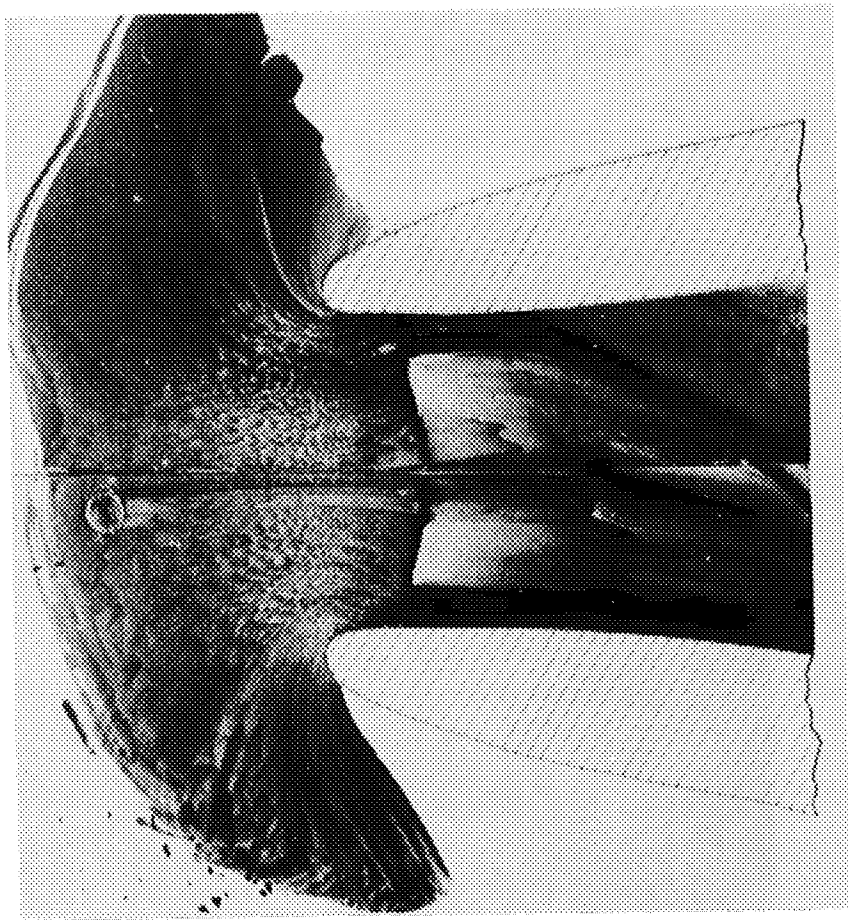

(c) NACA 1-40-200 nose inlet, m/m_s = choke.

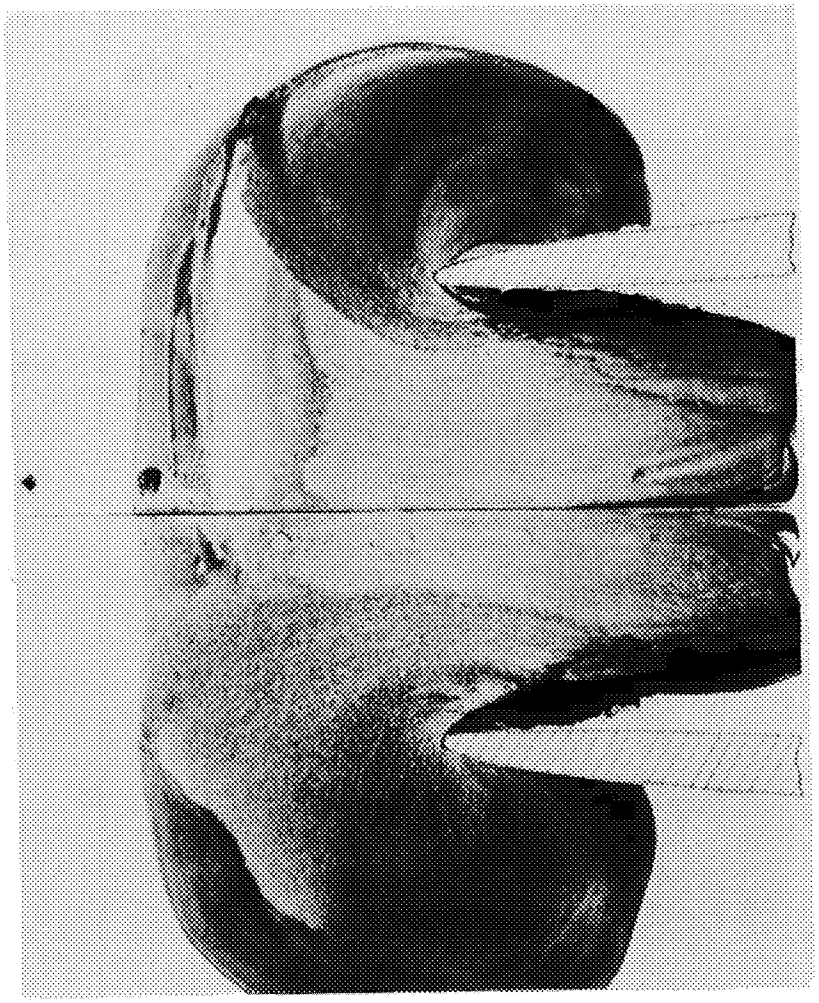

L-83682

(d) NACA 1-70-200 nose inlet, $m/m_s \approx 0.30$.

Figure 12.- Continued.

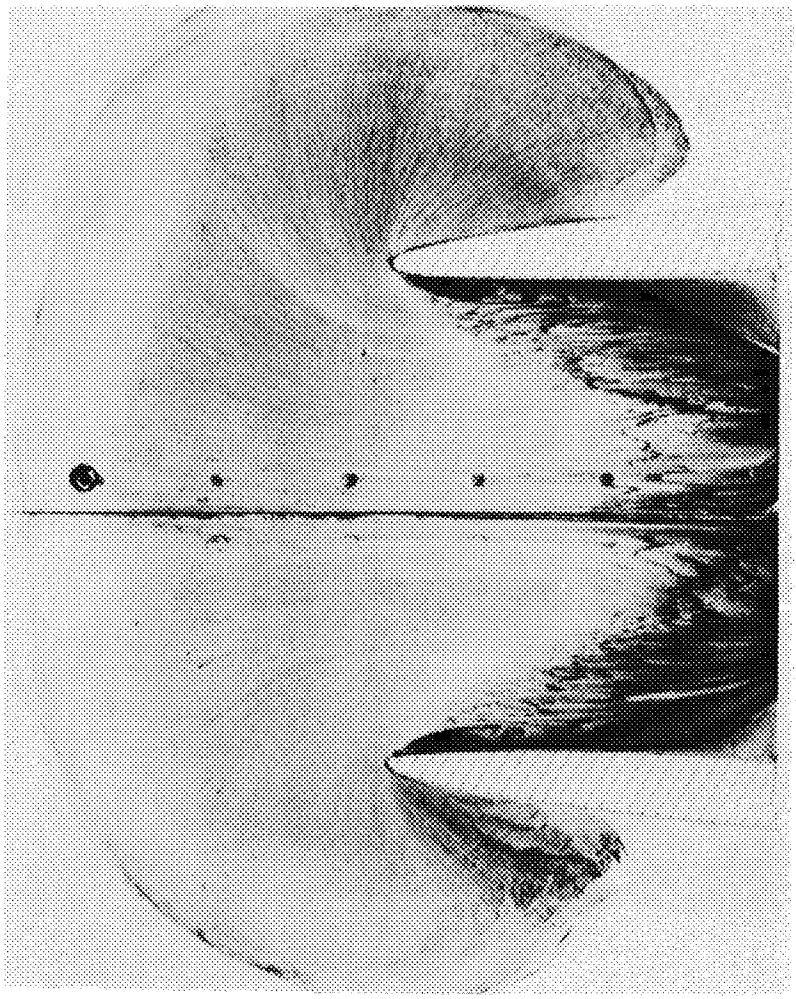

(e) NACA 1-70-200 nose inlet, $m/m_s \approx 0.33$.

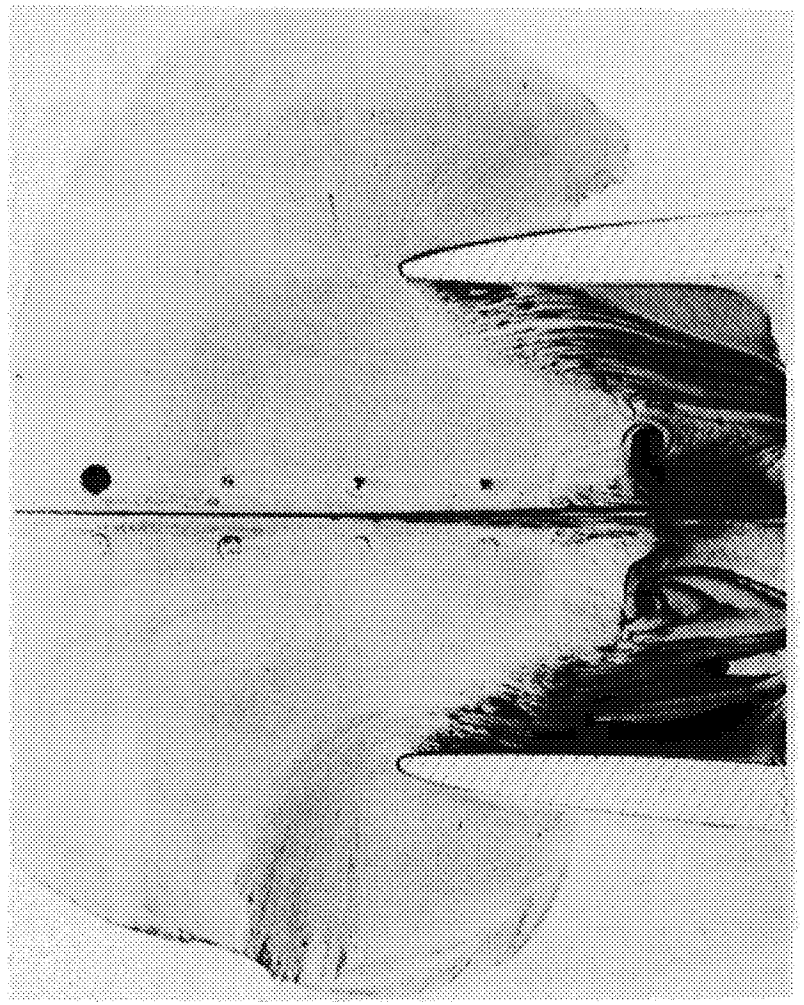

L-83683

(f) NACA 1-70-200 nose inlet, m/m_s = choke.

Figure 12.- Concluded.

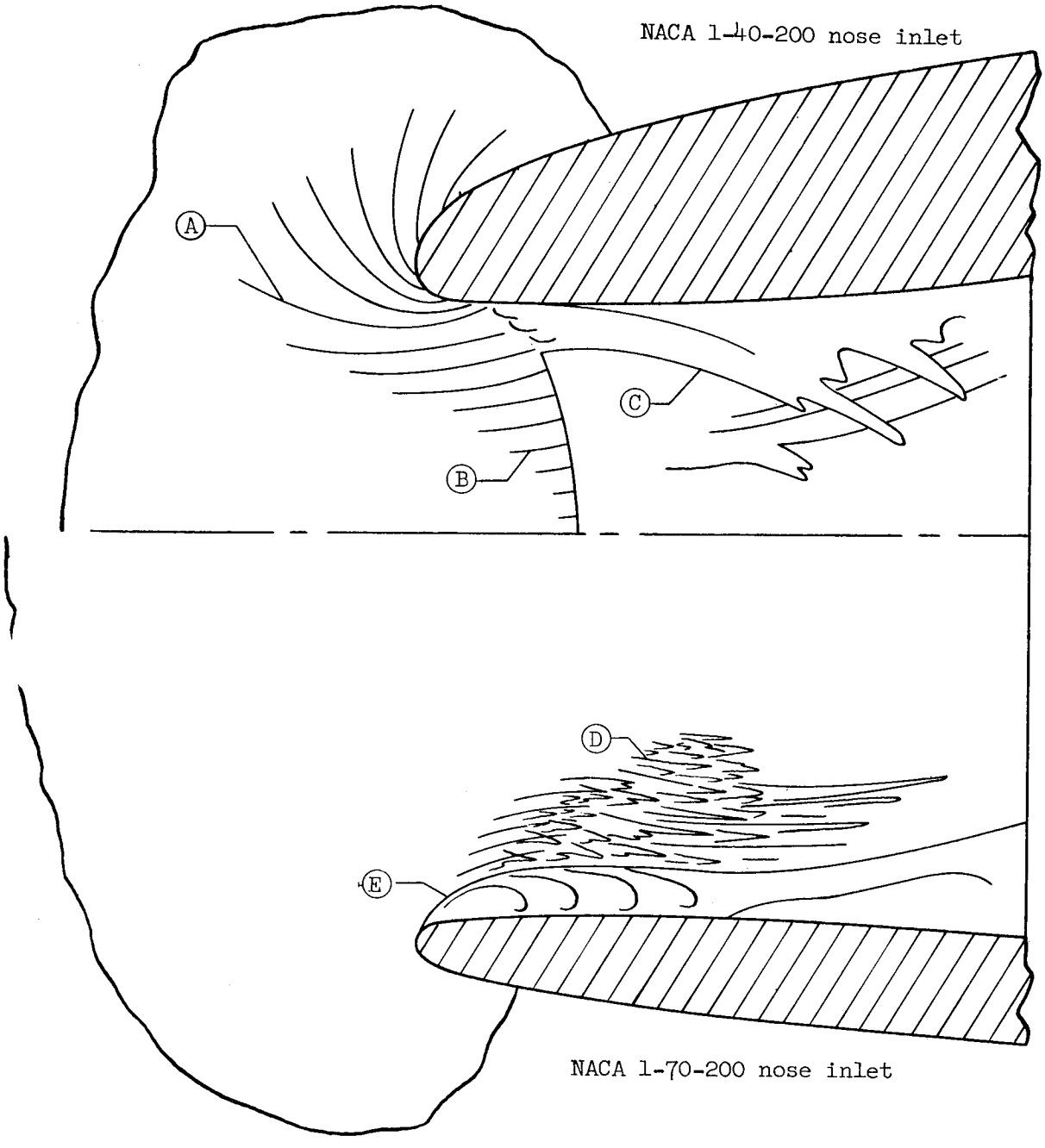

Figure 13.- Schematic drawing of types of phenomena observed in ink-flow photographs.

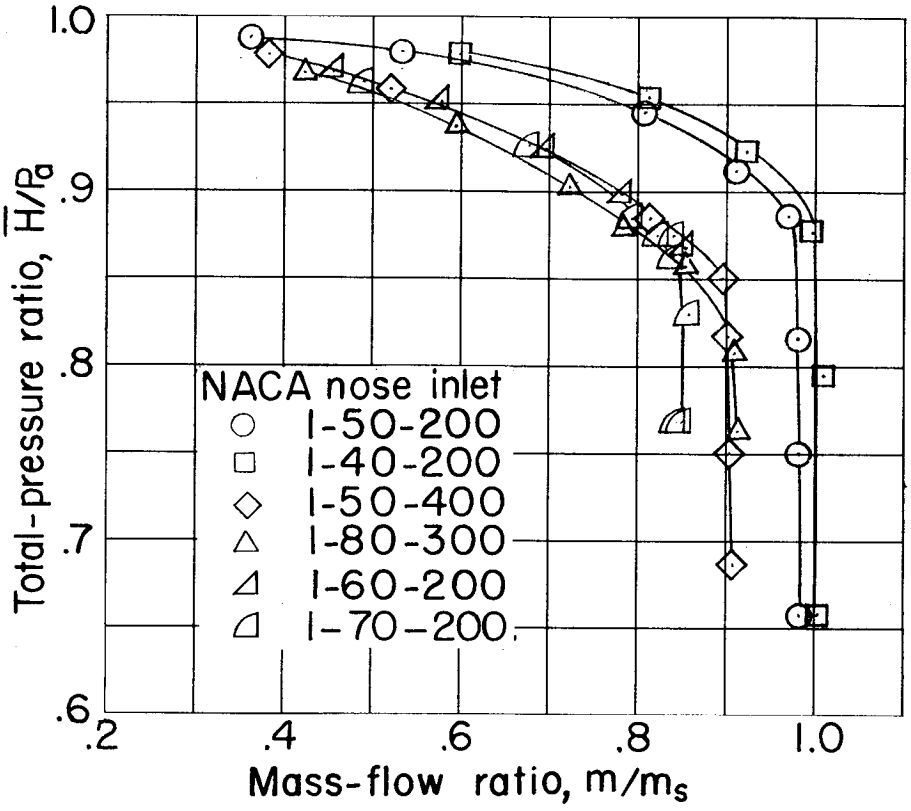

Figure 14.- Variation of average total-pressure ratio with mass-flow ratio.

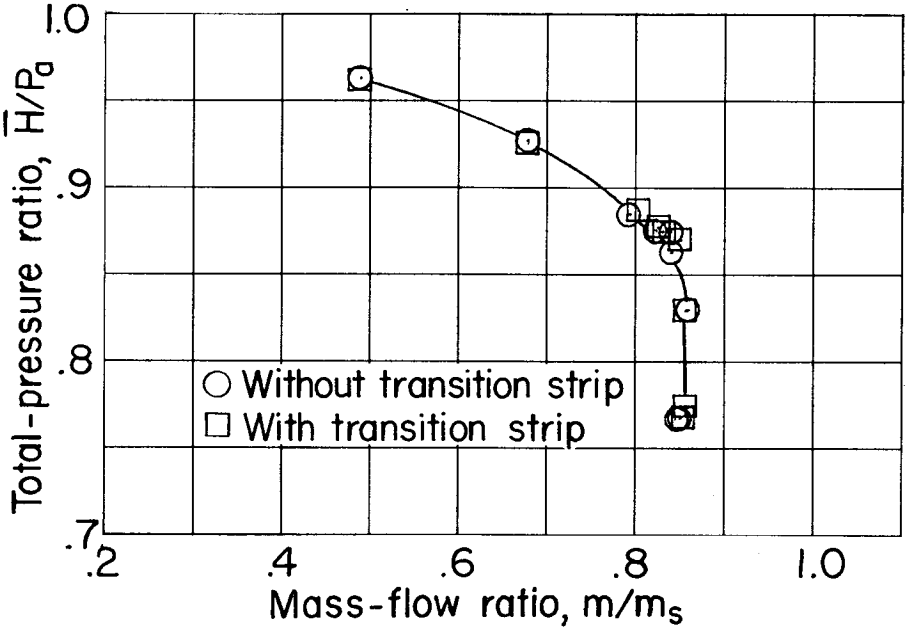

Figure 15.- Effect of transition strip on variation of total-pressure ratio with mass-flow ratio. NACA 1-70-200 nose inlet.

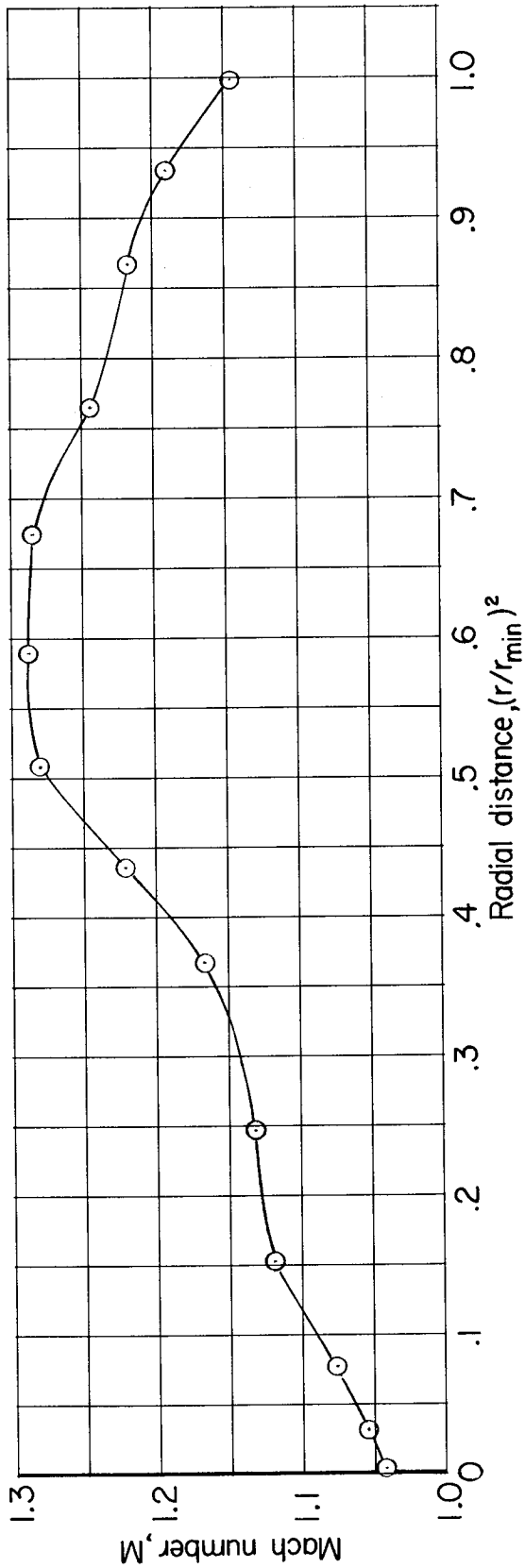

(a) Local Mach number.

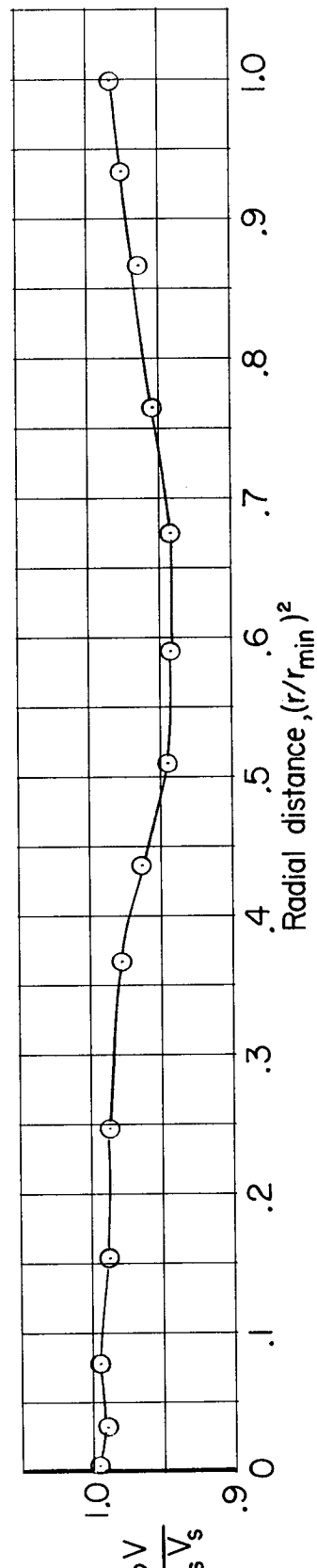

(b) Point mass-flow ratio.

Figure 16.- Results of survey of duct minimum-area station. NACA 1-50-200 nose inlet; total pressure is assumed to be P_a.

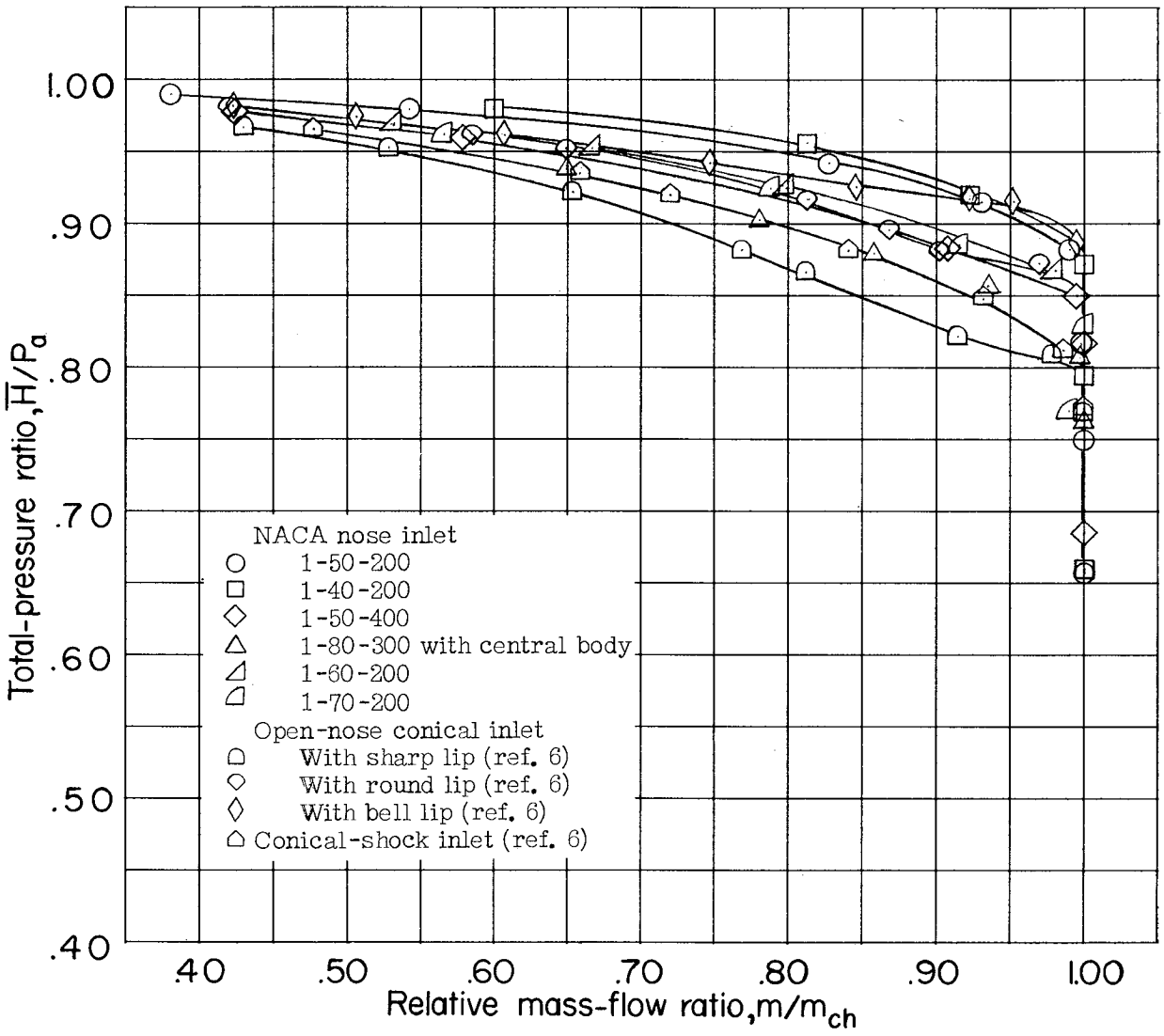

Figure 17.- Variation of average total-pressure ratio with relative mass-flow ratio.

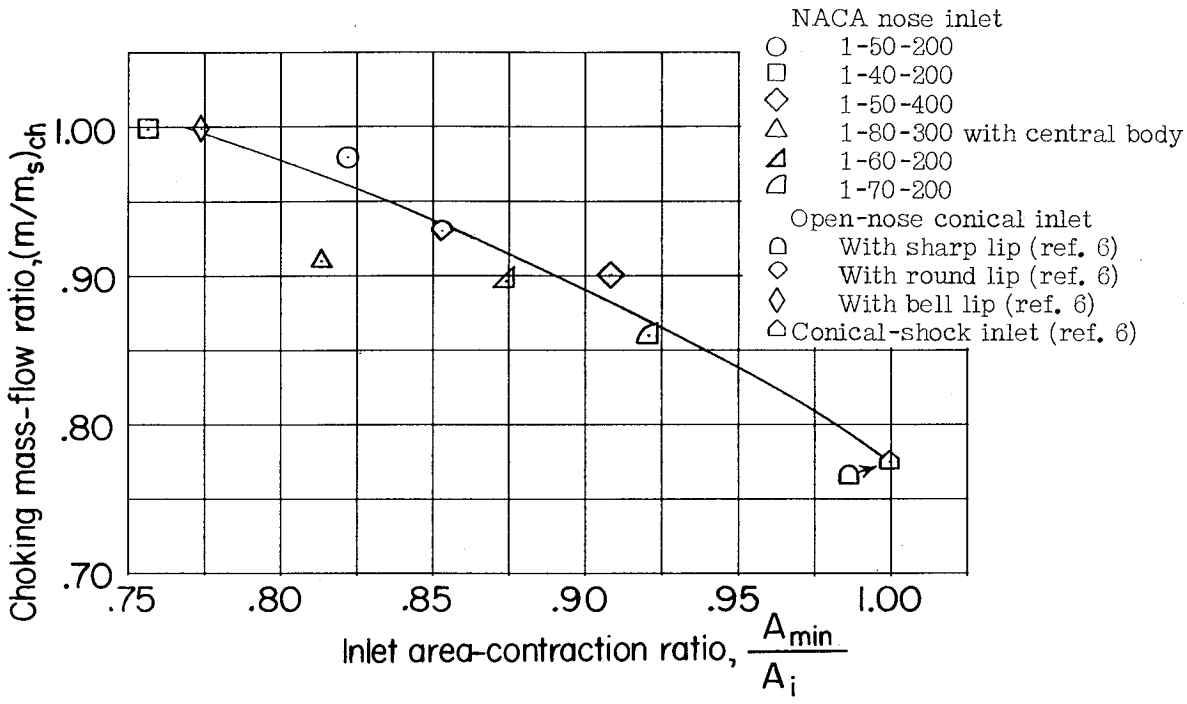

(a) Mass-flow ratio.

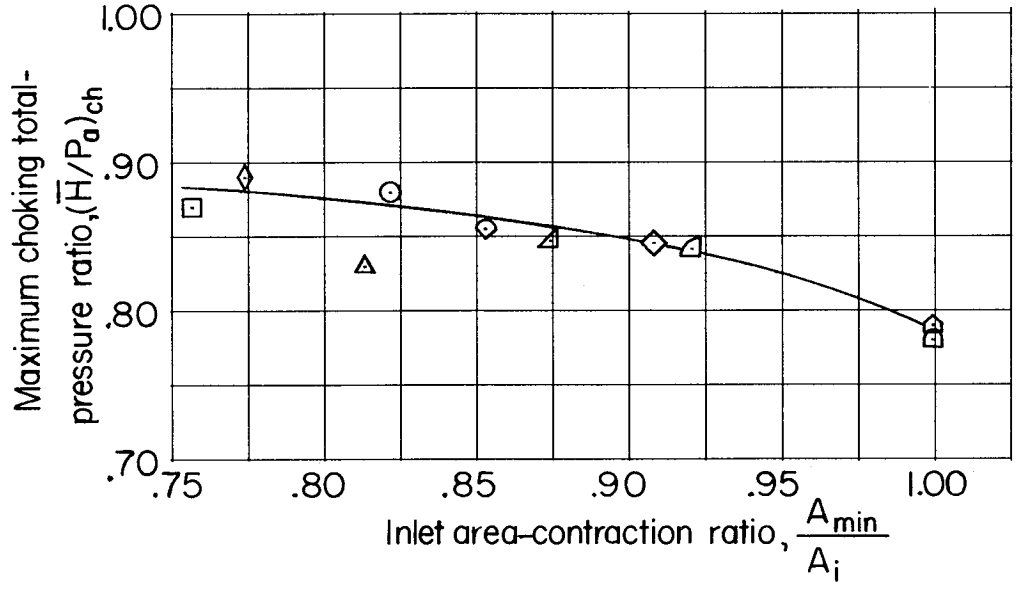

(b) Total-pressure ratio.

Figure 18.- Variation of maximum choking total-pressure ratio and choking mass-flow ratio with inlet-entrance area-contraction ratio.

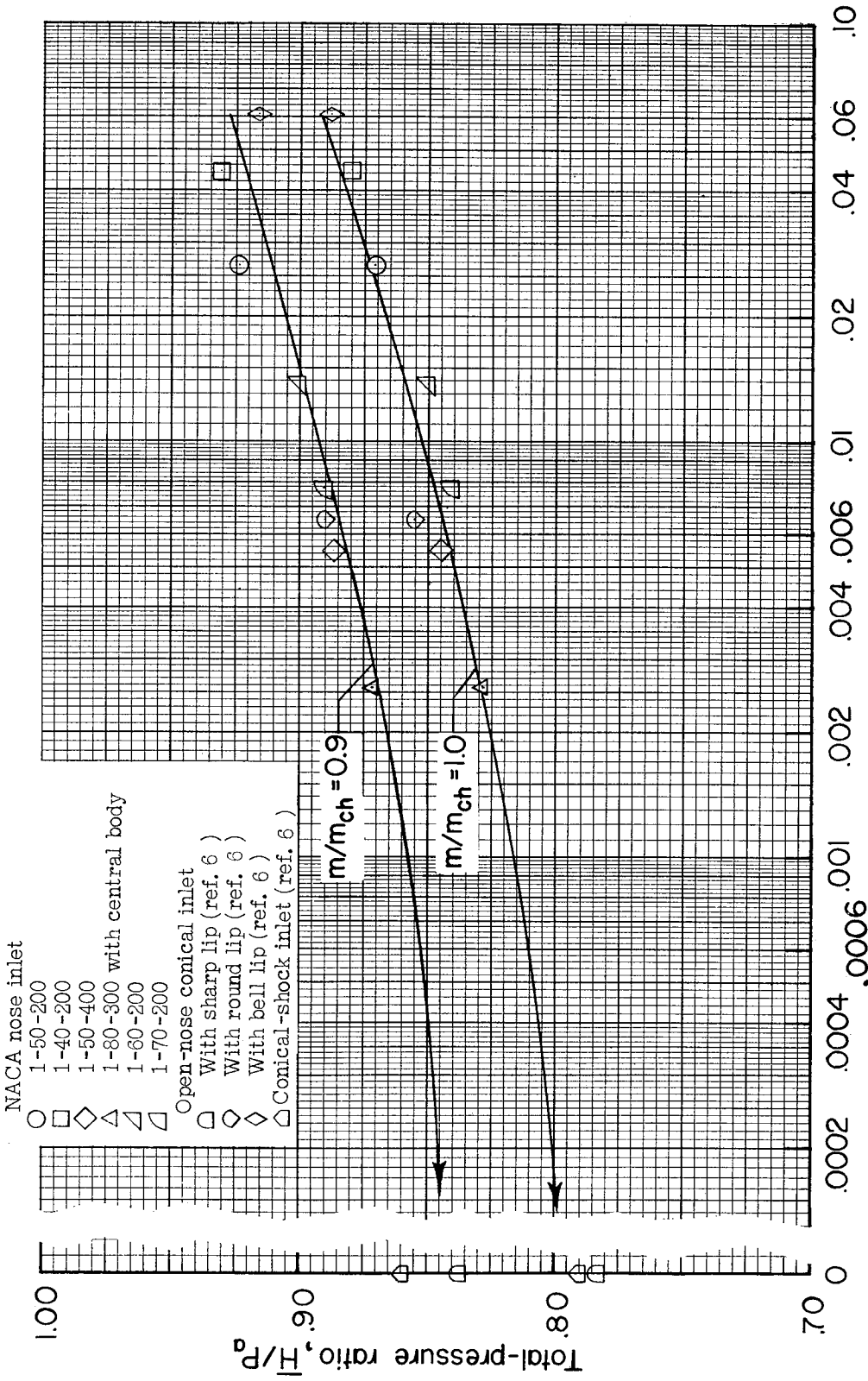

Figure 19.- Variation of average total-pressure ratio with the lip-roundness parameter $\frac{XY}{r_i^2}$.